DEVCOM
ARMY RESEARCH
LABORATORY

Progress on Zirconia-Polyurea Matrix Hybrid Composites

by Alex J Hsieh, Victor K Champagne, Steven E Kooi, and Christopher A Schuh

NOTICES

Disclaimers

The findings in this report are not to be construed as an official Department of the Army position unless so designated by other authorized documents.

Citation of manufacturer's or trade names does not constitute an official endorsement or approval of the use thereof.

Destroy this report when it is no longer needed. Do not return it to the originator.

ARMY RESEARCH
LABORATORY

Progress on Zirconia-Polyurea Matrix Hybrid Composites

Alex J Hsieh
Weapons and Materials Research Directorate, CCDC Army Research Laboratory
Institute for Soldier Nanotechnologies, Massachusetts Institute of Technology

Steven E. Kooi
Institute for Soldier Nanotechnologies, Massachusetts Institute of Technology

Victor K Champagne and Christopher A Schuh
Department of Materials Science and Engineering, Massachusetts Institute of Technology

REPORT DOCUMENTATION PAGE

Form Approved
OMB No. 0704-0188

1. REPORT DATE *(DD-MM-YYYY)*	2. REPORT TYPE	3. DATES COVERED (From - To)
December 2019	Technical Report	1 October 2018–29 August 2019

4. TITLE AND SUBTITLE	5a. CONTRACT NUMBER
Progress on Zirconia-Polyurea Matrix Hybrid Composites	
	5b. GRANT NUMBER
	5c. PROGRAM ELEMENT NUMBER
6. AUTHOR(S)	5d. PROJECT NUMBER
Alex J Hsieh, Victor K Champagne, Steven E Kooi, and Christopher A Schuh	
	5e. TASK NUMBER
	5f. WORK UNIT NUMBER

7. PERFORMING ORGANIZATION NAME(S) AND ADDRESS(ES)	8. PERFORMING ORGANIZATION REPORT NUMBER
CCDC Army Research Laboratory ATTN: FCDD-RLW-MG Aberdeen Proving Ground, MD 21005	ARL-TR-8867

9. SPONSORING/MONITORING AGENCY NAME(S) AND ADDRESS(ES)	10. SPONSOR/MONITOR'S ACRONYM(S)
	11. SPONSOR/MONITOR'S REPORT NUMBER(S)

12. DISTRIBUTION/AVAILABILITY STATEMENT

Approved for public release; distribution is unlimited.

13. SUPPLEMENTARY NOTES

ORCID ID(s): Alex J Hsieh , 0000-0003-0958-0390

14. ABSTRACT

In state-of-the-art ballistic body armor, laminate composites comprising ceramic plates with metallic and ultrahigh molecular weight polyethylene fiber composite backing layers using adhesives have the potential to achieve lightweight ballistic efficiency. Here, we aim to exploit shock impedance optimization at the bilayer interface, particularly between ceramic and adhesive layers. This study investigates the incorporation of zirconia particles into polyurea elastomers to form hybrid composites as a potential candidate structural adhesive material. Pristine zirconia particles are first thoroughly premixed with an oligomeric diamine, also a reactant for polyurea, as an alternative pathway without organosilanes for surface functionalization. Interface interactions between zirconia and polyurea in the matrix are revealed via attenuated total reflectance-Fourier transform infrared spectroscopy, where a shift and broadening of the urea–carbonyl stretching and an increase in relative intensity of the corresponding disordered versus ordered N–H stretching are shown in hybrid composites versus bulk polyurea. This corroborates well the presence of relaxation broadening in the tanδ data in dynamic mechanical analysis, where a shift of the soft phase glass transition toward higher temperatures is evidenced in hybrid composites in contrast to a well-defined segmental α relaxation observed in bulk material. The composition dependence of the dynamic storage modulus is also elaborated.

15. SUBJECT TERMS

zirconia-polyurea matrix hybrid composites, interfacial interaction, attenuated total reflectance-Fourier transform infrared spectroscopy, wide angle X-ray diffraction (WAXD), small angle X-ray scattering (SAXS), thermogravimetric analysis, dynamic mechanical analysis, segmental dynamics

16. SECURITY CLASSIFICATION OF:			17. LIMITATION OF ABSTRACT	18. NUMBER OF PAGES	19a. NAME OF RESPONSIBLE PERSON
					Alex J Hsieh
a. REPORT	**b. ABSTRACT**	**c. THIS PAGE**	UU	26	19b. TELEPHONE NUMBER (Include area code)
Unclassified	Unclassified	Unclassified			(410) 306-2292

Standard Form 298 (Rev. 8/98)
Prescribed by ANSI Std. Z39.18

Contents

List of Figures

Acknowledgments

1. Introduction

Hierarchical elastomers such as segmented polyureas,[1–6] poly(urethane urea)s,[7–16] and polyurethanes[17–20] typically consist of a combination of hard and soft segments, which often vary considerably in chemical structure. The evolution through self-association of hard segments, facilitated via strong intermolecular hydrogen bonding, would result in microphase separation and a complex microstructure. This class of elastomeric materials, as pointed out by Roland and coworkers,[1,2] could have potential to undergo a transient phase transition upon extreme dynamic loading conditions, from rubbery at ambient to become leathery or even glassy when the impulse approaches the respective segmental mobility. The discovery of this novel molecular mechanism was coined as high-rate, deformation-induced glass transition,[2] through which the potential toward enhanced energy absorption and dissipation was postulated.[1,2,21,22] Meanwhile, Hsieh et al. further elucidated that intersegment mixing between the soft phase and hard domains was essential toward enhanced dynamic stiffening, where a poly(urethane urea), PUU 532-1000, revealed moderate improvement in the resistance against impact by a 20-µm steel particle at strain rates of approximately $10^8 \, s^{-1}$, than a polyurea, PU 1000, despite both having approximately the same hard segment contents.[23] The variation in the extent of dynamic stiffening upon impact corroborated well the corresponding segmental dynamics. PUU 532-1000 exhibited a segmental α relaxation time associated with the soft phase, which was about four orders of magnitude slower than that of PU 1000, approximately 1.1×10^{-1} s versus approximately 2.2×10^{-5} s, determined at 25 °C by broadband dielectric relaxation spectroscopy.[23] Additionally, the segmental dynamics of the local β relaxation of PUU 532-1000 appeared to be very close to that of the segmental α relaxation of PU 1000, which was further indicative of greater intersegment mixing in PUU 532-1000 than PU 1000.[23] Furthermore, recent experimental observations obtained from select model two-component polyurethanes clearly elucidated the essence of molecular attributes toward dynamic stiffening, where a predominantly amorphous polyurethane exhibited greater dynamic stiffening than the corresponding semicrystalline counterpart.[24]

Meanwhile, advancements in high-performance fibers, inorganic fillers, nanoparticles, and carbon nanotubes have led to the development of lightweight polymer matrix composites for integration into design of a broad range of engineered structures and components used in automobiles, aircrafts, as well as lightweight military tactical vehicles.[25–30] In practice, organosilanes are utilized in surface modification of fibers or fillers to yield better dispersion, thereby mitigating agglomeration of these reinforcement materials.[31,32] Additionally, surface

1

modification can lead to proper interface interaction and subsequently adequate stress transfer between matrix and reinforcement in order to achieve the desired mechanical properties and performance characteristics of the composites. Zirconia (ZrO_2) is known to exhibit high hardness, stiffness, flexural strength, and fracture toughness, as well as a low coefficient of friction.[33,34] Additionally, recent research efforts revealed that addition of dopants such as ceria and yttria to zirconia had led to the development of unique characteristics such as shape memory or superelasticity, where stress-induced martensitic transformation was noted between tetragonal and monoclinic phases.[35–37] This transformation was observed in micron-sized, ceria-doped zirconia particles and was shown to be reproducible upon deformation over hundreds of cycles to strains up to approximately 4.7%.[38] There has been increased interests in the development of ZrO_2-based and ZrO_2-containing ceramics particularly with respect to their potential toward enhanced fracture toughness.[39]
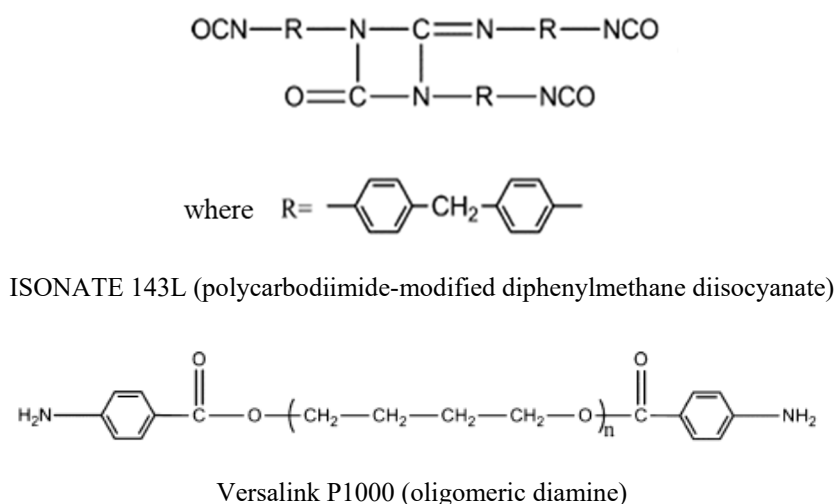
The motivation for this research is to exploit the intrinsic hardness of ZrO_2 along with the dynamic stiffening characteristics of hierarchical elastomers for integration into fabrication of hybrid composites for dynamic mechanical properties optimization. Recent progress has shown that incorporation of zirconia nanoparticles functionalized by 3-aminopropyltriethoxysilane led to a strong covalent bond with the epoxy-based matrix and subsequently greater interlaminar strength of the resultant fiber-reinforced, zirconia-modified epoxy matrix composites.[32] Successful silanization of zirconia nanoparticles was hypothesized as a result of the reaction of organosilanes with surface hydroxyl groups, which was attributed to the presence of strongly absorbed water from the atmosphere.[32] Meanwhile, it was also reported that the surface of zirconia contains a variety of catalytically active sites,[40] including Brønsted acidic and basic hydroxyl groups and coordinatively unsaturated Lewis acidic-base $Zr^{4+}O^{2-}$ pairs.[41] The presence of Lewis acidic sites was shown to be more abundant on the monoclinic phase,[41] and further, the nature of the zirconia phases strongly affected the adsorption of carbon monoxide (CO) and carbon dioxide (CO_2).[41] A higher CO_2 adsorption capacity of the monoclinic-ZrO_2 was attributed to the presence of a higher concentration and basicity of the hydroxyl groups on this polymorph, as well as the stronger Lewis acidity of Zr^{4+} cations and the stronger Lewis basicity of O^{2-} anions than the tetragonal counterpart.[41]

In this work, we undertake an interface design approach through exploring the inherent dipolar characteristics of pristine zirconia—whereby zirconia particles are thoroughly premixed with an oligomeric diamine, which is also a reactant for polyurea—as an alternative pathway to the aforementioned organosilane-based surface functionalization. This is followed by addition of diisocyanate into the

oligomeric diamine/zirconia mixture, where an in-situ polymerization/casting process encompasses completion of reaction along with the formation of zirconia/polyurea composites. We investigate the extent of dipolar interaction between zirconia and polyurea in the matrix, as well as their influence on the material characteristics of resultant hybrid composites.

2. Experimental

The bulk PU 1000 was prepared by reaction of poly(tetramethylene oxide di-*p*-aminobenzoate) (Versalink P1000, Evonik)[42] with a polycarbodiimide-modified diphenylmethane diisocyanate (ISONATE 143 L, Dow Chemical)[43] at a 4:1 weight ratio, as shown in Fig. 1. Undoped zirconia microparticles in the monoclinic phase (SF-EXTRA, Saint Gobain) were used in this study. A representative crystal structure of zirconia is shown in Fig. 2.[40] Meanwhile, characterization of particle-size distribution provided by Saint Gobain using a Microtrac–FRA9200 analysis showed the distribution to be $d_{10} = 0.441$ μm, $d_{50} = 0.889$ μm, and $d_{90} = 12.32$ μm. A two-step synthesis route was utilized in the fabrication of zirconia-polyurea matrix composites; zirconia particles were first premixed with oligomeric diamine and then followed by the addition of diisocyanate to the mixture. In each step, thorough mixing and degassing was ensured during processing; the mixture was then cast between glass plates to complete polymerization. The reaction and final consolidation of the mixtures were carried out in a vacuum oven, first at 25 °C for 8 h and then at 80 °C for additional 12 h, for both the bulk and hybrid composites.

ISONATE 143L (polycarbodiimide-modified diphenylmethane diisocyanate)

Versalink P1000 (oligomeric diamine)

Fig. 1   Chemical structure of ISONATE 143L[43] and Versalink P-1000 oligomeric diamine[6,42]
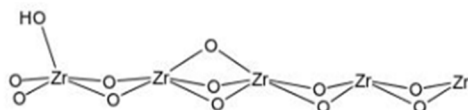
Fig. 2   Representative crystal structure of the zirconia surface

The attenuated total reflectance-Fourier transform infrared (ATR-FTIR) spectra were acquired with 512 scans at a resolution of 1 cm^{-1} using a Thermo Scientific Nicolet 6700 FT–IR with a diamond ATR cell.

Wide angle X-ray diffraction (WAXD) and small angle X-ray scattering (SAXS) measurements were carried out in a SAXSLAB (Xenocs) instrument with a DECTRIS PILATUS 300K detector. The system has a microbeam X-ray source ($\lambda = 1.54$ Å) as produced by Cu-Kα, and the voltage and current were set to 45 kV and 0.66 mA, respectively. The WAXD data are expressed in terms of intensity versus 2θ, where 2θ is the scattering angle, while SAXS data are based on the scattering vector q, where $q = 4\pi \sin(\theta)/\lambda$, λ is the wavelength of the incident radiation, and θ is one half the scattering angle.

Thermogravimetric analysis (TGA) measurements were carried out using a TA Instruments Discovery TGA, where specimens were heated at 20 °C/min up to 600 °C for determination of the residual weight upon combustion in air.

Dynamic mechanical analysis (DMA) data were obtained with a TA Instruments Q800 DMA at 1 Hz and 0.1% strain, from –120 to 100 °C at a heating rate of 2 °C/min.

3.   Results

3.1 Material Characteristics

We use the TGA measurements to determine the efficacy of a step-wise processing route for incorporation and mixing of zirconia microparticles into fabrication of hybrid composites. In Fig. 3, results from TGA reveal the presence of a two-step thermal degradation characteristic in the bulk as well as both zirconia composites, which is consistent with previously reported observations on the bulk polyurea (PU).[44] Meanwhile, it is noteworthy that all three materials exhibit the char formation after being heated to 600 °C in air. Results of the percentage weight (wt%) change obtained as a function of temperature are compared, as shown in Fig. 3, where the residual weight fraction is determined to be approximately 7.2%, 52.6%, and 59.8% for the bulk, hybrid 1, and hybrid 2, respectively. In comparison, the residual weight-percent data of the hybrid composites are comparable with the

composition of zirconia used in the corresponding PU hybrid composites, 50.3 and 58.1 wt%, respectively, given the fact that the extent of char associated with each PU matrix may vary. Meanwhile, the volume percent of the zirconia content calculated based on the initial composition is approximately 16.8% and 19.6% for hybrid 1 and hybrid 2, respectively, where the density of zirconia is taken as 5.68 g/cm^{3,45} and for the bulk PU is 1.09 g/cm^3, which was measured by following the buoyancy method.
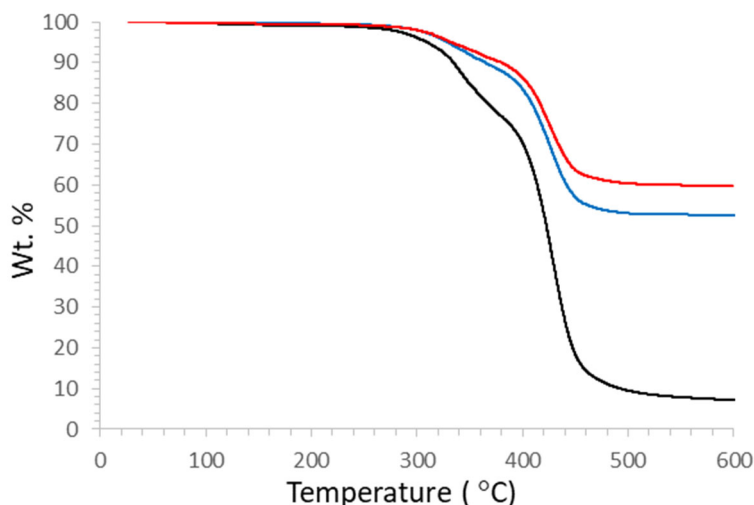
Fig. 3   Residual weight-percent as a function of temperature obtained from thermal degradation by TGA for PU 1000 bulk (black), PU hybrid 1 (blue), and PU hybrid 2 (red)

3.2 Interface-Induced Intermolecular Interaction

The state of hydrogen-bonding association measured by ATR-FTIR is used to discern whether interface interaction between the PU matrix and zirconia is plausible. Figure 4 compares the ATR-FTIR spectra obtained for the bulk PU 1000 and both hybrid 1 and hybrid 2 composites. Generally, the stretching modes of hydrogen-bonded N–H groups (ν(N–H)) and carbonyls (ν(C=O)) have distinct wavenumber assignments in the free, disordered, and ordered states.[6] For PU 1000, the ordered band of N–H stretching are predominantly associated with the aligned urea linkages in the hard domain phase, while the disordered bands as well as those associated with hydrogen-bonded ureas to the ether oxygen groups in polytetramethylene oxide (PTMO) were reported to arise from hydrogen bonds present in the mixed phase.[6] The stretching absorption bands of free, disordered, and ordered hydrogen-bonded N–H groups are observed at approximately 3460, 3360, and 3303 cm^{-1}, respectively, consistent with previously reported data.[6] Meanwhile, the carbonyl bands are observed at approximately 1711 and 1642 cm^{-1} for the free ester-carbonyls[46] and ordered hydrogen-bonded urea-carbonyl moieties, respectively.[6]
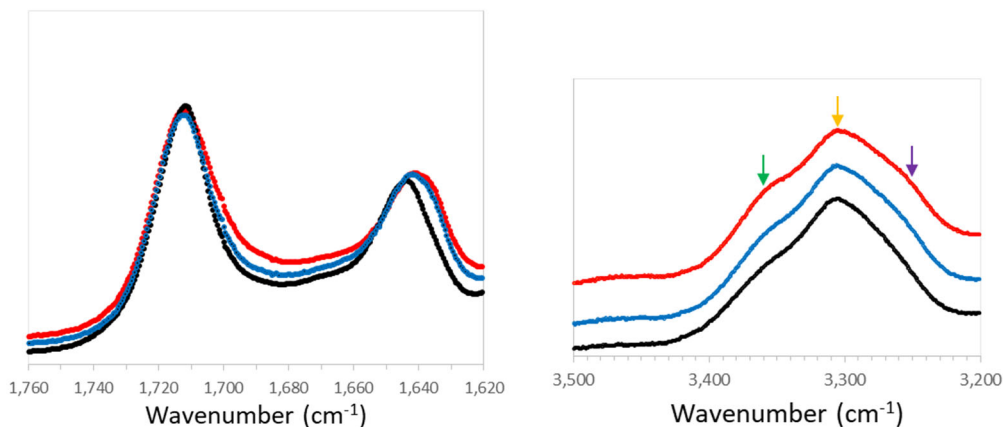
Fig. 4   ATR-FTIR spectra obtained for a) the carbonyl stretching regions and b) the N−H stretching regions of the bulk PU 1000 (black), hybrid 1 (blue), and hybrid 2 (red); arrows in b) point to the ordered (orange) and disordered (green) stretching, as well as ether oxygen stretching (purple) regions

It is envisioned that zirconia could act as a Lewis acid[41] as well as a hydrogen-bond donor by the presence of $[Zr^{4+}O^{2-}]$ and $[Zr\text{-}OH]$, respectively, for participating in intermolecular interaction via dipolar or hydrogen bonding with the carbonyls of the urea moieties in the matrix. As a result, the carbonyls stretching reveals a slight shift of the peak frequency associated with the hydrogen-bonded ureas to lower wavenumbers, where the spectra become broadened as the zirconia content increases, in comparison to that of the bulk PU. This is in contrast to the ester-carbonyl stretching, which remains unchanged among the bulk and both hybrid composites. Meanwhile, the broadening of the urea-carbonyl stretching could be related to the heterogeneity of the zirconia-polyurea composites, where the carbonyls are interacting with zirconia to various degrees. Correspondingly, it is apparent that for the hybrid composites the relative intensity of the disordered versus the ordered N–H stretching increases, presumably as a result of the monodentate hydrogen-bond formation due to the presence of zirconia interaction, rather than the bidentate urea–urea linkage predominantly seen in the bulk. Meanwhile, a weak shoulder at approximately 3260 cm^{-1} is noted in the hybrids, which is presumably due to the hydrogen-bond formation between the amide protons of urea and the ether oxygen moieties in PTMO. These observations are strongly indicative that an interface interaction is present between the PU matrix and zirconia, even without addition of any organosilane surfactants.

6

3.3 Evolution of Microstructure

The influence of zirconia incorporation on the microstructure was examined by SAXS and WAXD measurements. In SAXS, the variation in the scattering intensity profiles is shown in Fig. 5, where PU 1000 exhibits a broad scattering peak. The mean interdomain spacing (d), calculated based on the peak maxima (q_{max}), where q is the scattering vector and d = $2\pi/q_{max}$, is ∼7 nm, which is consistent with the reported data.[6] Meanwhile, addition of zirconia microparticles results in a considerable change in the scattering, which becomes significantly broadened and indistinct, as shown in Fig. 5 for the hybrid 1 composite, presumably reflecting the influence of a broad range of the particle-size distribution in zirconia.
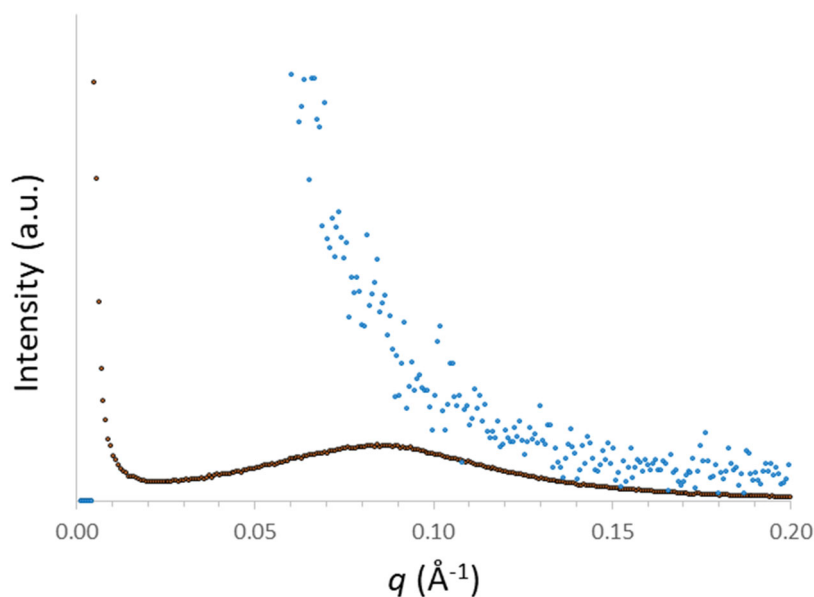
Fig. 5   **SAXS profiles of PU 1000 (black) and hybrid 1 composite (blue)**

The WAXD data, shown in Fig. 6, reveal the presence of an amorphous halo at approximately 19.6° for the bulk PU 1000. This amorphous halo is also observed in hybrid 1 at a similar 2θ; however, its intensity is moderately decreased. For hybrid 2, the amorphous halo becomes relatively insignificant. This trend in the amorphous halo intensity corroborates well with the variation in the extent of disordered versus ordered hydrogen-bonded N–H stretching observed in ATR-FTIR for both hybrid composites than that of the bulk, as shown in Fig. 4. Meanwhile, there are additional diffraction peaks present in both hybrid 1 and hybrid 2, at 2θ of approximately 17.4°, 24.0°, 28.0°, and 31.3°, which are consistent with the diffraction peaks associated with the crystal structure of zirconia, also shown in Fig. 6.

Fig. 6   WAXD profiles of PU 1000 (black), hybrid 1 (blue), hybrid 2 (red), and zirconia powder (green)

3.4 Dynamic Mechanical Relaxation Measurements

We are particularly interested in the influence of zirconia incorporation that could affect the viscoelastic relaxation associated with the matrix elastomer, PU 1000. Figure 7 is a plot of the storage modulus as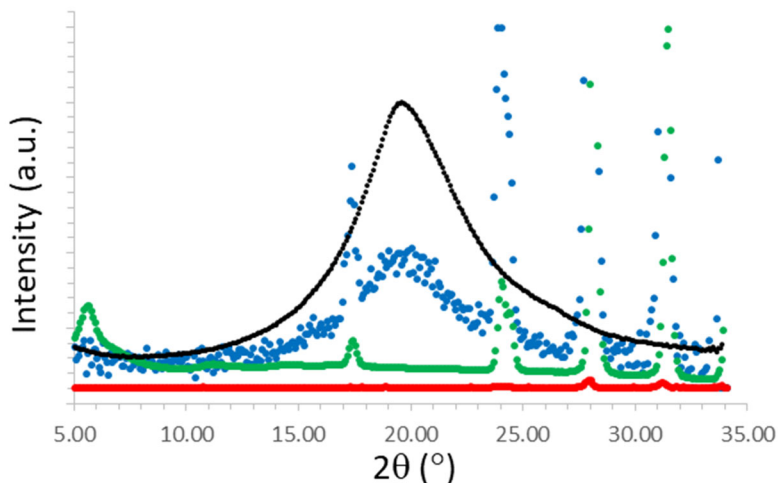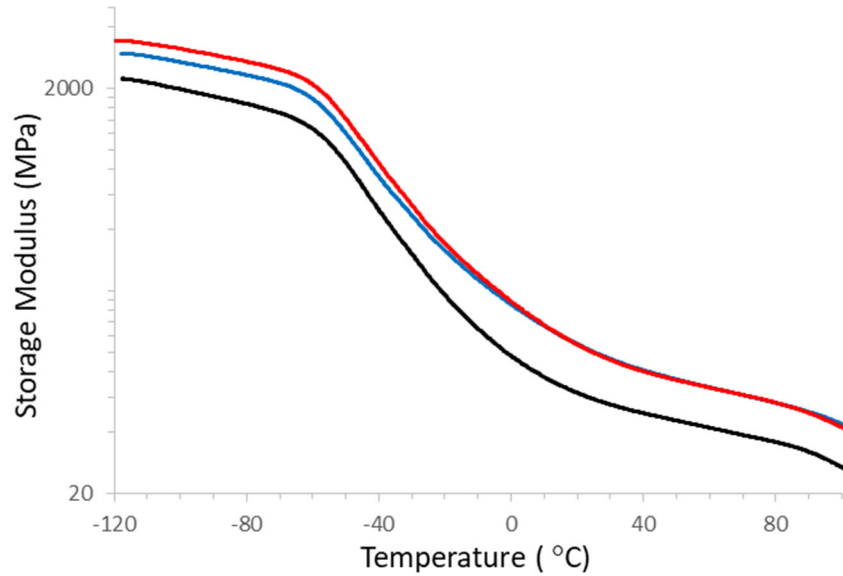 a function of temperature obtained at 1 Hz via DMA for PU 1000 and both zirconia-hybrid composites. Incorporation of zirconia clearly results in an increase in the storage modulus of both hybrid composites compared to that of the bulk, where the ambient rubbery storage modulus is about the same for both hybrid composites, approximately 99–100 MPa versus approximately 58 MPa for the bulk. Additionally, there is an appreciable difference revealed as temperature decreases and reaches approximately 5 °C and over the rubber-to-glass transition region. For comparison, the glassy storage modulus determined at –80 °C is approximately 2713 MPa for PU hybrid 2, which is higher than that of PU hybrid 1 and the bulk, approximately 2329 and 1679 MPa, respectively. Meanwhile, the loss modulus data show the presence of a distinct segmental α relaxation, T_g, at a temperature of approximately –50 °C (not shown), corresponding to the T_g of the soft phase in PU 1000, which is consistent with the previously reported data.[6]

It is noteworthy that for hybrid composites the tanδ data reveal the presence of a significant broadening of the soft phase glass transition toward higher temperatures, in contrast to a well-defined segmental α relaxation observed in the bulk, as shown in Fig. 8. We hypothesize that the broadening could be facilitated through a strong interface interaction, via either dipolar or hydrogen-bond interaction, between the PU matrix and the surface of zirconia microparticles. While addition of zirconia has shown to result in a decrease in the relaxation intensity in both hybrid

8

composites than the bulk, partly as a result of less matrix material participating in the glass transition, the hybrid 2 composite nevertheless reveals a slight increase in the tanδ loss factor than hybrid 1 over the broad soft phase glass transition region. This trend in the broadened relaxation corroborates well the variation in relative intensity of the disordered versus the ordered N–H stretching as well as the shift and broadening associated with the corresponding urea-carbonyl stretching, revealed via ATR-FTIR as shown in Fig. 4.

Fig. 7   The temperature dependence of storage modulus data obtained at 1 Hz via DMA for PU 1000 bulk (black), PU hybrid 1 (blue), and PU hybrid 2 (red)
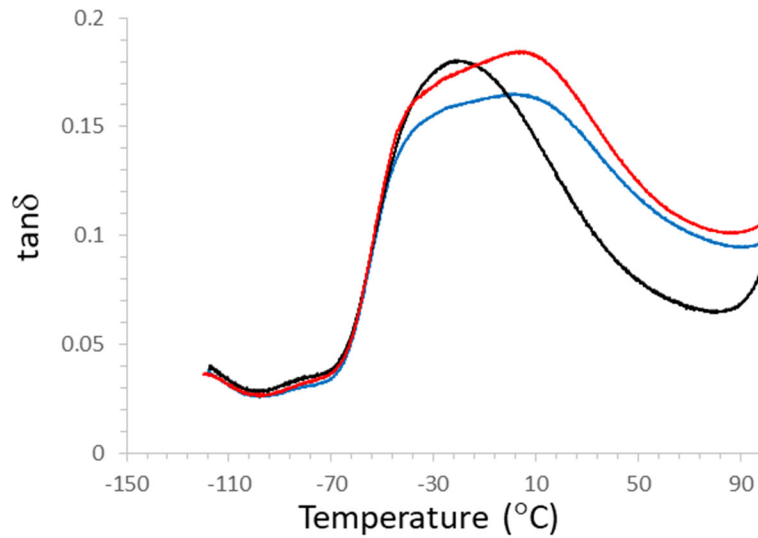

Fig. 8   DMA tan δ data obtained at 1 Hz for PU 1000 bulk (black), PU hybrid 1 (blue), and PU hybrid 2 (red)

4. Discussion

In hybrid composites, as the filler content increases, one of the common characteristics is that many polymer chains are in close contact with reinforced fillers, where the confinement effects on matrix elastomers have been well studied.[47–49] Meanwhile, it was reported that immobilization of polymer chains near the interface could affect the chain dynamics and potentially induce glassy behavior of interfacial chains at temperature above the T_g of the bulk polymer.[47]

Here, we investigate whether enhanced interactions noted between zirconia and PU in the matrix, which appears to disrupt the propensity of urea moieties to form ordered bidentate hydrogen-bond interaction, could also be an attribute to the variation in the dynamic storage modulus of matrix elastomers observed in hybrid composites. For better illustration, Fig. 9 compares the normalized storage modulus data, based on the ratio of the respective modulus of each hybrid composite versus the bulk, as a function of temperature. It is noteworthy that the normalized storage modulus data look very similar over the ambient temperature range, yet a deviation is noted that commences at a temperature approximately between –5 and 5 °C, and becomes significant as the temperature further decreases. This inception temperature range is very close to the onset temperature of the rubber-to-glass transition of the bulk PU 1000, as shown in Fig. 10, which was previously determined by broadband dielectric relaxation spectroscopy measurement.[23] These observations corroborate well the trend in the broadening of segmental α relaxation, as shown in Fig. 8, which indirectly validates the influence of interface interaction that could affect the matrix dynamics of PU 1000 in zirconia hybrid composites. Further, we hypothesize that the shift of soft phase glass transition to higher temperatures is a plausible attribute to a significant increase in sub-T_g dynamic storage modulus of matrix elastomer in hybrid 1 as compared to hybrid 2.
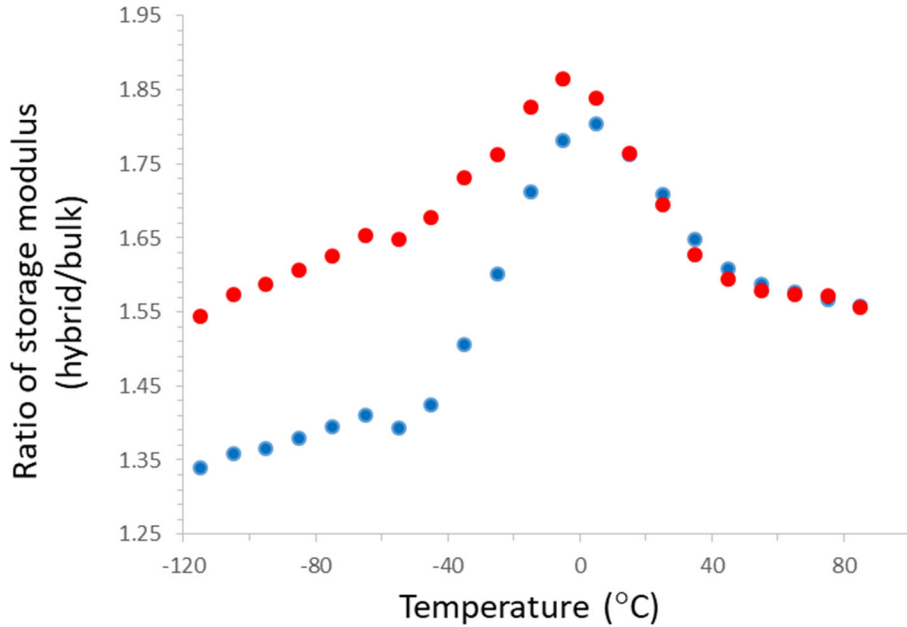
Fig. 9 **Comparison of the ratio of storage modulus (hybrids/bulk) data obtained at 1 Hz via DMA for PU hybrid 1 (blue) and PU hybrid 2 (red)**
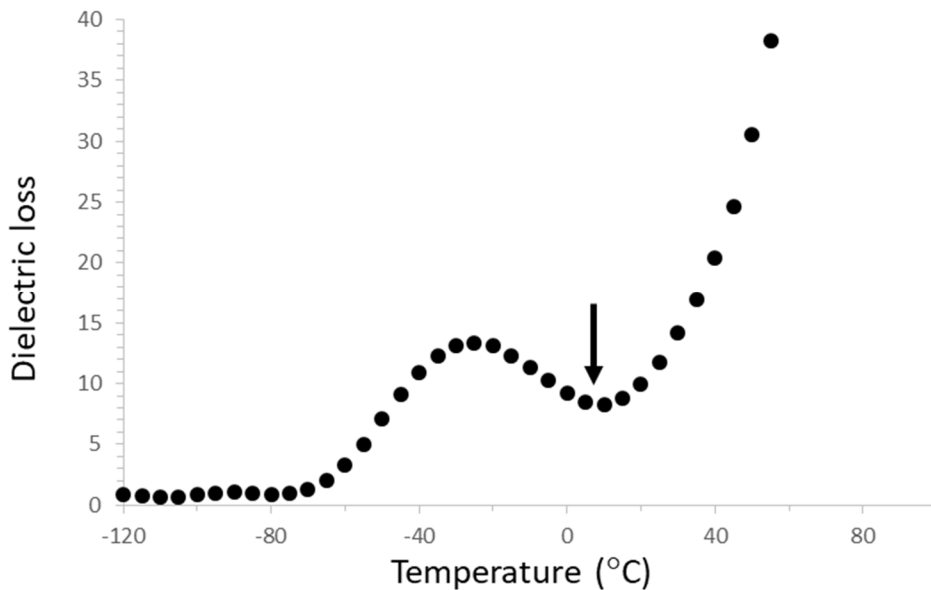
Fig. 10 **Broadband dielectric relaxation data of the isochronal dielectric loss obtained at 1 Hz as a function of temperature for PU 1000 (arrow points to the onset temperature of rubber-to-glass transition)**

Meanwhile, the relaxation broadening phenomenon observed as a result of enhanced interface interaction in zirconia PU 1000 hybrid composites resembles the molecular influence on the segmental α relaxation observed via DMA in the aforementioned PUU 532-1000 versus PU 1000, as shown in Fig. 11, where the

11

extent of intersegment mixing is significantly greater in PUU 532-1000 than PU 1000.
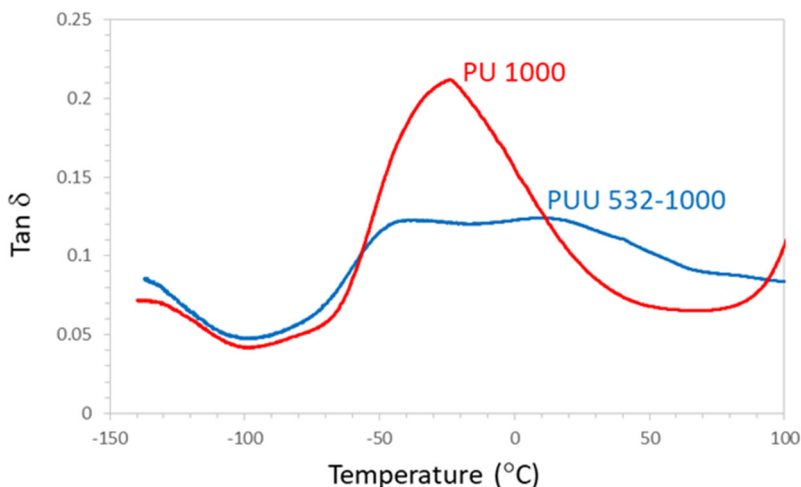

Fig. 11   DMA tan δ data obtained at 1 Hz for PUU 532-1000 (blue) and PU 1000 (red)

5.   Conclusion

We have demonstrated a plausible pathway where the use of an oligomeric diamine is effective to first facilitate dispersion of zirconia particles, followed by the completion of in-situ polymerization to form zirconia-polyurea matrix hybrid composites. This process route is greatly desired, as there is no need of organosilanes for surface functionalization of zirconia nor the use of any solvent for compounding of zirconia-polyurea mixtures.

We hypothesize that addition of zirconia microparticles could potentially interfere the bidentate urea–urea linkage formation, presumably facilitated through interface interaction via hydrogen bonding. This would presumably promote intersegment hydrogen bonding between the dispersed hard segments and the neighboring soft segments. Enhanced interface interaction is evidenced by the presence of relaxation broadening along with an increase in the relative intensity of the tanδ data in DMA, as well as a shift and broadening of the carbonyl stretching in ATR-FTIR, as the zirconia content increases in hybrid composites.

Meanwhile, it is envisioned that a synergistic effect involving stress-induced martensitic transformation in zirconia along with a transient high-rate deformation-induced rubber-to-glass transition in a PU matrix elastomer could lead to the enhanced dynamic stiffening and strengthening characteristics required for protection against extreme dynamic environments.

6. References

1. Roland CM, Casalini R. Effect of hydrostatic pressure on the viscoelastic response of polyuria. Polymer. 2007;48:5747–52. doi:10.1016/j.polymer.2007.07.017.

2. Bogoslovov RB, Roland CM, Gamache RM. Impact-induced glass transition in elastomeric coatings. Appl Phys Lett. 2007;90:221910. doi:10.1063/1.2745212.

3. Fragiadakis D, Gamache R, Bogoslovov RB, Roland CM. Segmental dynamics of polyurea: effect of stoichiometry. Polymer. 2010;51:178–84. doi:10.1016/j.polymer.2009.11.028.

4. Castagna AM, Fragiadakis D, Lee H-K, Choi T, Runt J. The role of hard segment content on the molecular dynamics of poly(tetramethylene oxide)-based polyurethane copolymers. Macromolecules. 2011;44:7831–36. doi:10.1021/ma2017138.

5. Choi T, Fragiadakis D, Roland CM, Runt J. Microstructure and segmental dynamics of polyurea under uniaxial deformation. Macromolecules. 2012;45:3581−3589. doi:10.1021/ma300128d.

6. Castagna AM, Pangon A, Choi T, Dillon GP, Runt J, The role of soft segment molecular weight on microphase separation and dynamics of bulk polymerized polyureas. Macromolecules. 2012;45:8438-44. doi:10.1021/ma3016568.

7. Sarva SS, Hsieh AJ. The effect of microstructure on the rate-dependent stress-strain behavior of poly(urethane urea) elastomers. Polymer. 2009;50(13):3007-3015. doi:10.1016/j.polymer.2009.04.025.

8. Strawhecker KE, Hsieh AJ, Chantawansri TL, Kalcioglu ZI, Van Vliet KJ. Influence of microstructure on micro-/nano-mechanical measurements of select model transparent poly(urethane urea) elastomers. Polymer. 2013;54:901-908. doi:10.1016/j.polymer.2012.12.018.

9. Hsieh AJ, Chantawansri TL, Hu W, Strawhecker KE, Casem DT, Eliason JK, Nelson KA, Parsons EM. New insight into microstructure-mediated segmental dynamics in select model poly(urethane urea) elastomers. Polymer. 2014;55:1883–92. doi:10.1016/j.polymer.2014.02.037.

10. Rinaldi RG, Hsieh AJ, Boyce MC. Tunable microstructures and mechanical deformation in transparent poly(urethane urea)s. J Polym Sci Part B Polym Phys. 2011;49:123–35. 10.1002/polb.22128.

11. Chantawansri TL, Sliozberg YR, Andzelm JW, Hsieh AJ. Coarse-grained modeling of model poly(urethane urea)s: Microstructure and interface aspects. Polymer. 2012;53(20):4512-24. doi: 10.1016/j.polymer.2012.07.056.

12. Veysset D, Hsieh AJ, Kooi SE, Maznev AA, Masser KA, Nelson KA. Dynamics of supersonic microparticle impact on elastomers revealed by real-time multi-frame imaging. Sci Rep. 2016;6:25577. doi:10.1038/srep25577.

13. Veysset D, Hsieh AJ, Kooi SE, Nelson KA. Molecular influence in high-strain-rate microparticle impact response of poly(urethane urea) elastomers. Polymer. 2017;123:30–38. doi.org/10.1016/j.polymer.2017.06.071.

14. Sheth JP, Aneja A, Wilkes GL, Yilgor E, Atilla GE, Yilgor I, Beyer FL. Influence of system variables on the morphological and dynamic mechanical behavior of polydimethylsiloxane based segmented polyurethane and polyurea copolymers: A comparative perspective. Polymer. 2004:45;6919–32. doi:10.1016/j.polymer.2004.06.057.

15. Yilgor E, Isik M, Yilgor I. Novel synthetic approach for the preparation of poly(urethaneurea) elastomers. Macromolecules. 2010;43:8588–93. doi:10.1021/ma101770k.

16. Fragiadakis D, Runt J. Molecular dynamics of segmented polyurethane copolymers: Influence of soft segment composition. Macromolecules. 2013;46:4184–90. doi:10.1021/ma4006395.

17. Korley LTJ, Pate BD, Thomas EL, Hammond PT. Effect of the degree of soft and hard segment ordering on the morphology and mechanical behavior of semicrystalline segmented polyurethanes. Polymer. 2006;47:3073–82. doi:10.1016/j.polymer.2006.02.093.

18. Hsieh AJ, Chantawansri TL, Hu W, Cain J, Yu JH. New insight into the influence of molecular dynamics of matrix elastomers on ballistic impact deformation in UHMWPE composites. Polymer. 2016;95:52–61. doi:10.1016/j.polymer.2016.04.048.

19. Cooper SL, Tobolsky AV. Properties of linear elastomeric polyurethanes. J Appl Poly Sci. 1966;10:1837–44. doi:10.1002/app.1966.070101204.

20. Wang CB, Cooper SL. Morphology and properties of segmented polyether polyurethaneureas. Macromolecules. 1983;16:775–86. doi:10.1021/ma00239a014.

21. Porter JR, Dinan RJ, Hammons MI, Knox KJ. Polymer coatings increase blast resistance of existing and temporary structures. AMPTIAC Quarterly. 2002;6(4):47–52.

22. Barsoum RG. Elastomeric polymers with high rate sensitivity: applications in blast, shockwave, and penetration mechanics. 1st ed. Norwich (NY): William Andrew Publisher; 2015.

23. Hsieh AJ, Veysset D, Miranda DF, Kooi SE, Runt J, Nelson KA. Molecular influence in the glass/polymer interface design: the role of segmental dynamics. Polymer. 2018:146;222–229. doi:10.1016/j.polymer.2018.05.034.

24. Wu YCM, Hu W, Sun Y, Veysset D, Kooi SE, Nelson KA, Swager TM, Hsieh AJ. Unraveling the high strain-rate dynamic stiffening in select model polyurethanes – the role of intermolecular hydrogen bonding. Polymer. 2019;1168:218–227. doi:10.1016/j.polymer.2019.02.038.

25. Lubin G. Handbook of composites. New York (NY): Van Nostrand Reinhold; 1982.

26. Dresselhaus MG, Dresselhaus G, Eklund PC. Science of fullerenes and carbon nanotubes. New York (NY), San Diego (CA): Academic Press; 1996.

27. Winey KI, Vaia RA. Polymer nanocomposites. MRS Bull. 2007;32:314–9.

28. Thomas EL, National Research Council. Opportunities in protection materials science and technology for future army applications. Washington (DC): The National Academies Press; 2011.

29. Wardle BL. Nanocomposites and nano-engineered composites reinforced with aligned carbon nanotubes. In: Proceedings ICCM-17 of the 17th International Conference on Composite Materials; 2009 July; Edinburgh, UK.

30. Silvestre J, Silvestre N, de Brito J. An overview on the improvement of mechanical properties of ceramics nanocomposites. J Nanomaterials. 2015; doi:10.1155/2015/106494.

31. Ishida H, Koenig JL. Fourier-transform infrared spectroscopic study of structure of silane coupling agent on E-glass fiber. J Colloid Interface Sci. 1978;64:565–576. doi:10.1016/0021-9797(78)90399-5

32. Halder S, Ahemad S, Das S, Wang J. Epoxy/glass fiber laminated composites integrated with amino functionalized ZrO2 for advanced structural applications. ACS Appl Mater Interfaces. 2016;8:1695−1706. doi: 10.1021/acsami.5b09149.

33. Somiya S. Handbook of advanced ceramics: materials, applications, processing, and properties. 2nd ed. New York (NY): Academic Press; 2013. doi:10.1016/B978-0-12-385469-8.01001-7.

34. Silvestre J, Silvestre N, de Brito J. An overview on the improvement of mechanical properties of ceramics nanocomposites. J Nanomaterials. doi: 10.1155/2015/106494.

35. Reyes-Morel PE, Chen IW. Transformation plasticity of CeO2-stabilized tetragonal zirconia polycrystals: I, stress assistance and autocatalysis. J Am Ceram Soc. 1988;71:343–353.

36. Reyes-Morel PE, Cherny JS, Chen IW. Transformation plasticity of CeO2-stabilized tetragonal zirconia polycrystals: II, pseudoelasticity and shape memory effect. J Am Ceram Soc. 1988;71:648–657.

37. Zeng XM, Du Z, Schuh CA, Tamura N, Gan CL. Microstructure, crystallization and shape memory behavior of titania and yttria co-doped zirconia. Journal of the European Ceramic Society. 2016;36:1277–1283.

38. Du Z, Ye P, Zeng XM, et al. Synthesis of monodisperse CeO2–ZrO2 particles exhibiting cyclic superelasticity over hundreds of cycles. J Am Ceram Soc. 2017;100:4199–4208. https://doi.org/ 10.1111/jace.14972.

39. Du Z, Yu HZ, Schuh CA. Inventors. Shape memory ceramic particles and structures formed thereof. United State patent application. WO2017/139706 A1. 2017 Aug 17.

40. Surface properties of transition metal oxides. Wikimedia Inc.; 2019 Feb 22 [accessed 2019 Sep 11]. https://en.wikipedia.org/wiki/Surface_properties_ of_transition_metal_oxides

41. Pokrovski K, Jung KT, and Bell AT. Investigation of CO and CO2 adsorption on tetragonal and monoclinic zirconia. Langmuir. 2001;17(14):4297–4303.

42. Versalink P-1000. Oligomeric diamine, product information. Essen (Germany): Evonik; 2019.

43. ISONATE 143L−modified MDI, product information. Midland (MI): Dow Chemical; 2019.

44. Awad WH, Wilkie CA. Investigation of the thermal degradation of polyurea: the effect of ammonium polyphosphate and expandable graphite. Polymer. 2010;51(11):2277-85. doi: https://doi.org/10.1016/j.polymer.2010.03.033.

45. Zirconium dioxide. Wikimedia Inc.; 2019 June 9 [accessed 2019 Sep 11]. https://en.wikipedia.org/wiki/Zirconium_dioxide.

46. Yilgor I, Yilgor E, Wilkes GL. Critical parameters in designing segmented polyurethanes and their effect on morphology and properties: A comprehensive review. Polymer. 2015; 58:A1–A36; doi:10.1016/j.polymer.2014.12.014.

47. Bogoslovov RB, Roland CM, Ellis AR, Randall AM, Robertson CG. Effect of silica nanoparticles on the local segmental dynamics in poly(vinyl acetate). Macromolecules. 2008;41:1289–96.

48. Berriot J, Montes H, Lequeux F, Long D, Sotta P. Evidence for the shift of the glass transition near the particles in silica-filled elastomers. Macromolecules. 2002;35:9756–62.

49. Montes H, Lequeux F, Berriot J. Influence of the glass transition temperature gradient on the nonlinear viscoelastic behavior in reinforced elastomers. Macromolecules. 2003;36:8107–18.

List of Symbols, Abbreviations, and Acronyms

ATR	attenuated total reflectance
DMA	dynamic mechanical analysis
FTIR	Fourier transform infrared spectroscopy
PTMO	polytetramethylene oxide
PU	polyurea
PUU	poly(urethane urea)
SAPI	small arms protective insert
SAXS	small angle X-ray scattering
TGA	thermogravimetric analysis
UHMWPE	ultrahigh molecular weight polyethylene
WAXD	wide angle X-ray diffraction
ZrO_2	zirconia

1 (PDF)	DEFENSE TECHNICAL INFORMATION CTR DTIC OCA
1 (PDF)	CCDC ARL FCDD RLD CL TECH LIB
1 (PDF)	CCDC ARL FCDD RLW MG AJ HSIEH